Synthesis of Uniform Rare Earth Fluoride ($NaMF_4$) Nanotubes by *In Situ* Ion Exchange from Their Hydroxide [$M(OH)_3$] Parents

Fan Zhang and Dongyuan Zhao*

Department of Chemistry, Shanghai Key Laboratory of Molecular Catalysis and Innovative Materials, and Laboratory of Advanced Materials, Fudan University, Shanghai 200433, People's Republic of China

ABSTRACT In this article, we demonstrate the production of uniform hexagonal sodium rare earth fluoride (β-$NaMF_4$) nanotubes through a hydrothermal *in situ* ion-exchange reaction by using rare earth hydroxides [$M(OH)_3$] as a parent. The trivalent rare earth hydroxides were hydrothermally prepared at 120 °C and possessed a quasi-layered structure, which could be formed to be nanotubal morphology through a rolling up process from 2-D sheets. Moreover, the hexagonal structure of rare earth hydroxides [$M(OH)_3$] displays a noticeable similarity with β-$NaMF_4$. This similarity makes the formation of β-$NaMF_4$ with nonlayered structure possible through *in situ* chemical transformation from $M(OH)_3$ with a layered structure. The single-crystal β-$NaMF_4$ nanotubes were synthesized with well-controlled diameter (80−500 nm), aspect ratio (6−30), wall thickness (25−80 nm), and contents (such as M = Pr, Sm, Gd, Tb, Dy, Er, as well as lanthanide-doped rare earth $NaMF_4$). The multicolor upconversion fluorescence has also been successfully realized in the Yb^{3+}/Er^{3+} (green) and Yb^{3+}/Tm^{3+} (blue) co-doped β-$NaMF_4$ nanotubes by UC excitation in the NIR region. The various UC emission ratios of the samples were investigated as a function of hydrothermal reaction time to research the UC properties of the products and to further demonstrate the hydrothermal *in situ* ion-exchange process.

KEYWORDS: hydrothermal · *in situ* ion exchange · upconversion · rare earth fluoride

One-dimensional (1-D) nanoscale materials, such as nanowires and nanotubes, have attracted much interest due to their importance in basic scientific research and potential technological applications.[1] They are expected to play an important role as both interconnects and functional components in the fabrication of nanoscale electronic and optoelectronic devices. Many unique and fascinating properties have already been proposed or demonstrated for the kind of materials, such as high luminescence efficiency,[2] superior mechanical toughness,[3] enhancement of thermoelectric figure of merit,[4] and a lowered lasing threshold.[5] However, among the low-dimensional luminescence nanomaterials, significant efforts have been mainly focused on the wide band gap emission in semiconductors such as Si,[6] Ge,[7] GaN,[8] InAs,[9] and ZnO.[2] More recently, upconversion (UC) luminescent materials[10] with unique antistokes optical property have garnered considerable attention due to their potential use as luminescence nanodevices ranging from solid-state lasers,[10] display monitors,[11] optical data storage,[10] fluorescence imaging for detection of biomolecules,[12] and optical-fiber-based telecommunications.[10] Up to now, colloidal nanocrystals of UC rare earth fluorides doped with lanthanides have also been obtained through sol−gel process,[13] co-precipitation,[14] organometallic approaches,[15,16] and hydrothermal methods.[17,18] However, few studies have focused on the synthesis of rare earth fluoride nanostructures with hollow interiors[18−20] because the preparation of rare earth fluoride nanotubes with nonlayered structure still remains challenging.

It was believed previously that, for the inorganic materials, only the substances with layered lattices could form nanotubes under appropriate conditions.[21−23] Well-defined inorganic nanotubes made of graphite, hexagonal boron nitrides, metal dichlorides, and sulfides, all possessing layered or pseudolayered structures, have successfully been produced without the assistance of templates.[21−23] Compared with layered compounds, the formation of nanotubes from nonlayered solids requires much more effort to bring together atoms or small particles into hollow cylinders in the process of crystallization. As a result, the preparation of nanotubes from nonlayered materials is often subjected to the use of templates such as CNTs (carbon nanotubes),[24] nanowires,[21] and porous membranes.[25] Although the sacrificial

*Address correspondence to dyzhao@fudan.edu.cn.

Received for review August 25, 2008 and accepted December 01, 2008.

Published online December 10, 2008. 10.1021/nn800533v CCC: $40.75

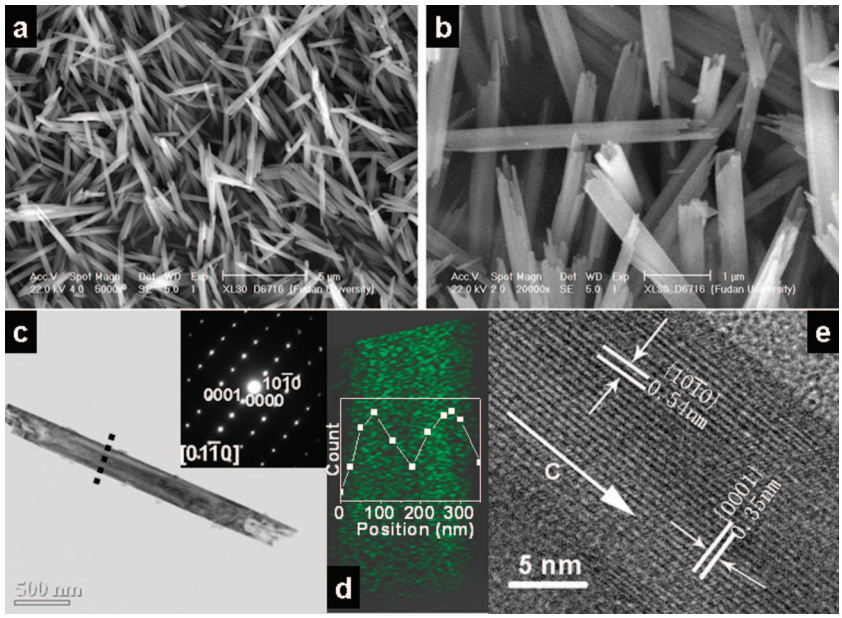

Figure 1. (a,b) SEM images of $Y(OH)_3$ nanotubes prepared at hydrothermal condition at 120 °C. (c) TEM image of the $Y(OH)_3$ nanotubes and corresponding ED pattern (inset). (d) Y compositional map of the nanotube obtained by energy dispersive spectroscopy, along with its intensity profile across the tube along the dotted line in (c). (e) HRTEM image of a $Y(OH)_3$ nanotube.

templating method has been proved to be a facile and efficient approach for the growth of tubular structures,[21,24] the structural disruption of the final product could not be avoided during the templates removing processes.[21] Most recently, a method based on an *in situ* chemical reaction in nanocrystals has also been developed to yield many hollow nanostructures.[26] However, the example for tubular structures especially for rare earth metal components has not been reported.

Here we report the production of hexagonal rare earth fluoride (β-$NaMF_4$) nanotubes through a hydrothermal *in situ* ion-exchange reaction with rare earth hydroxides [$M(OH)_3$] as a parent. The trivalent rare earth hydroxides, which possess a quasi-layered structure, could form the tubular nanostructure.[27,28] Moreover, the hexagonal structure of [$M(OH)_3$] displays a noticeable similarity with that of β-$NaMF_4$, which makes the formation of β-$NaMF_4$ with nonlayered structure possible through *in situ* ion-exchange transformation. The single-crystal β-$NaMF_4$ nanotubes can be synthesized with well-controlled diameter (80−500 nm), aspect ratio (6−30), wall thickness (25−80 nm), and contents (such as M = Pr, Sm, Gd, Tb, Dy, Er, Y, as well as lanthanide-doped rare earth $NaYF_4$). The multicolor UC fluorescence has also been successfully realized in the Yb^{3+}/Er^{3+} (green) and Yb^{3+}/Tm^{3+} (blue) co-doped β-$NaYF_4$ nanotubes by UC excitation in the NIR region.

RESULTS AND DISCUSSION

Rare earth hydroxides [$M(OH)_3$] can be synthesized under a hydrothermal condition from an aqueous solution of rare earth nitrate and NaOH.[27,28] Taking $Y(OH)_3$ as a example, scanning electron microscopy (SEM) images show that as-synthesized $Y(OH)_3$ nanotubes are uniform with smooth faceted surface (Figure 1a,b). The outer diameters are about 250 nm, and the wall thickness is about 30 nm. The lengths of the tubes are up to several micrometers. Transmission electron microscopy (TEM) images also reveal that the $Y(OH)_3$ products obtained from the hydrothermal condition show tubular morphologies (Figure 1c). The elemental map of the tube obtained by energy dispersive spectroscopy (EDS) also shows a characteristic intensity profile of Y element with the highest intensity observed at the edges (Figure 1d), further suggesting a tubular structure. HRTEM images recorded along the [010] zone axis clearly show that the tubes have a multiwall structure (Figure 1e), which is in accordance with the quasi-layered structure of $Y(OH)_3$ nanotubes.[27,28] The interlayer spacing is measured to be 0.54 and 0.35 nm corresponding to the {10$\bar{1}$0} and {0001} planes of $Y(OH)_3$ nanotubes (Figure 1e). The electron diffraction (ED) pattern (Figure 1c, inset) recorded perpendicular to the long axis of the single nanotube can be indexed to the [01$\bar{1}$0] zone axis of the hexagonal $Y(OH)_3$ structure with single-crystal feature XRD patterns of as-synthesized $Y(OH)_3$ nanotubes further revealing that the products are pure hexagonal $Y(OH)_3$ phase (space group of $P6_3/m$) with lattice constants a = 6.261 Å′ and c = 3.544 Å′ (JCPDS 83-2042) (Figure 2).

The tubular β-$NaYF_4$ can be prepared by hydrothermal *in situ* ion-exchange reaction of $Y(OH)_3$ nanotubes in the presence of diluted HF and NaF solution under the hydrothermal condition at 120 °C for 12 h. The yield is close to 100% according to the Y contents, suggest-

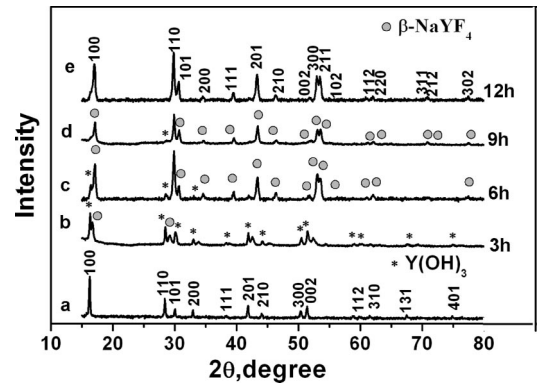

Figure 2. Powder XRD patterns of the as-synthesized $Y(OH)_3$ nanotube products (a) and the $Y(OH)_3/NaYF_4$ composite samples prepared through hydrothermal *in situ* ion-exchange transformation approach with different time: (b) 3 h, (c) 6 h, and (d) 9 h at 120 °C, (e) pure β-$NaYF_4$ obtained by the F-substituted reaction at 120 °C for 12 h.

ing an anion exchange process without dissolving metal ions. XRD patterns (Figure 2) show that the products are pure hexagonal $NaYF_4$ phase (space group $P6_3/m$) with lattice constants $a = 5.991(5)$ Å′ and $c = 3.620(1)$ Å′ (JCPDS 16-334). SEM images show that the samples prepared under hydrothermal condition at 120 °C for 12 h are uniform tube-like products, much similar to that of $Y(OH)_3$ tube parents, suggesting a replica process. The $NaYF_4$ nanotubes have an average diameter of 300 nm, wall thickness about 50 nm, and lengths of up to several micrometers (Figure 3a). In comparison to that of $Y(OH)_3$ nanotube parents, the outer diameter and the wall thickness increase slightly, which is ascribed to the lattice constant changes. TEM images display typical tubular particles contrasted with areas close to the edges (Figure 3b,c). The elemental map of the tubes obtained by energy dispersive spectroscopy (EDS) also shows a characteristic intensity profile of Y and F elements, respectively (Figure 3d,e). The highest intensity is observed at the position of the edges, providing further evidence for uniform β-$NaYF_4$ tubular structure with homogeneous element distribution. The highly dispersed F element also demonstrates that the hydrothermal *in situ* F-substituted reaction is realized homogeneously with $Y(OH)_3$ tubes as a template. The ED pattern (Figure 3b) taken from the side face of the nanotubes can be indexed as a hexagonal $NaYF_4$ single crystal along the $[01\bar{1}0]$ zone axis. Also, HRTEM images show an interplanar spacing of ~0.52 and 0.34 nm corresponding to the $\{10\bar{1}0\}$ and {0001} planes of β-$NaYF_4$ nanocrystals, respectively, further confirming that the [0001] plane is a preferred growth direction for the nanotubes.[27,28]

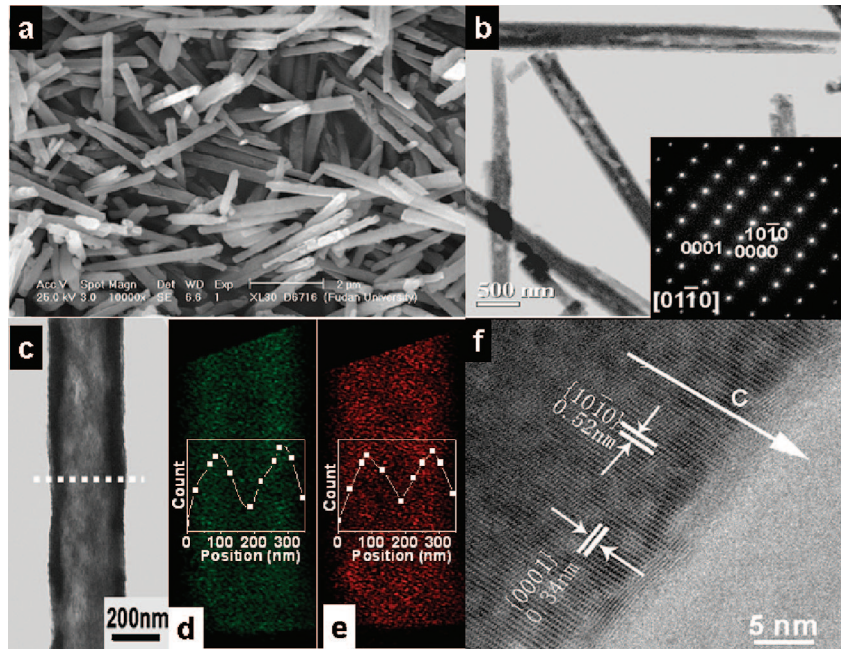

Figure 3. (a) SEM images of $NaYF_4$ nanotubes. (b) TEM image of the β-$NaYF_4$ nanotubes and corresponding ED patterns (inset). (c) TEM image of a single β-$NaYF_4$ nanotube. (d,e) Y and F compositional maps of the nanotube obtained by energy dispersive spectroscopy, along with its intensity profile across the tube along the dotted line in (c). (f) HRTEM image of a β-$NaYF_4$ nanotube.

XRD patterns show typical diffraction peaks corresponding to both $Y(OH)_3$ and β-$NaYF_4$ (Figure 2), clearly demonstrating that the hydrothermal *in situ* ion-exchange process occurs. As shown in Figure 2, the tube-like $Y(OH)_3$/β-$NaYF_4$ composites emerged after 3 h hydrothermal treatment in the presence of NaF and HF solution, and the $Y(OH)_3$ nanotubes could completely transform into β-$NaYF_4$ at 120 °C for 12 h. When the temperature increases to 200 °C, XRD patterns (Supporting Information, Figure S1a) show that the pure β-$NaYF_4$ phase can be obtained for 3 h, but SEM images (Supporting Information, Figure S2) reveal that most of the tube-like products appear to transform into nanorods under such high temperature. Our results show that the tube-like β-$NaYF_4$ products cannot be yielded when the temperature is below 100 °C even with a long reaction time (72 h). XRD results (Supporting Information, Figure S1b) show that the products are composites of YF_3 (JCPDS 74-0911) and a small quantity of cubic $NaYF_4$ (α-$NaYF_4$) (JCPDS 77-2042). When the reaction is carried out in the absence of HF, but only NaF, the pure β-$NaYF_4$ is also not obtained even at a temperature of 230 °C for more than 12 h (Supporting Information, Figure S1c). In the present work, the size of β-$NaYF_4$ nanotubes can be tuned by varying that of $Y(OH)_3$ parents. The outer diameter of the β-$NaYF_4$ tubes can be tuned from 80 to 500 nm, and the aspect ratio is changed from 6 to 300 nm and the wall thickness from 25 to 80 nm, respectively (Supporting Information, Figure S3).

XRD patterns reveal that pure hexagonal β-$NaYF_4$: Yb, Er/Tm samples are obtained with $Y(OH)_3$: Yb, Er/Tm nanotubes as a parent (Supporting Information, Figure S4). SEM and TEM images show that β-$NaYF_4$: 20% Yb, 2% Er and β-$NaYF_4$: 20% Yb, 2% Tm with uniform shape and size can be synthesized with the hydrothermal *in situ* ion-exchange route (Supporting Information, Figure S5). The results suggest that the doped ions have little effect on the morphology and size. Our results show that other rare earth $NaMF_4$ nanostructures such as M = Pr, Sm, Gd, Tb, Dy, and Er can also be produced by using the hydrothermal *in situ* ion-exchange route. (Supporting Information, Figure S6 and Table S1). It is demonstrated the outer diameters of $NaMF_4$ (M = Pr, Sm, Gd, Tb, Dy, and Er) nanotubes are variable from 55 to 110 nm at the same reaction condition, dependent on rare earth element's unit cell volume (Supporting Information, Table S1), which is related to lanthanide contraction. As shown in Figure S7 in the Supporting Infor-

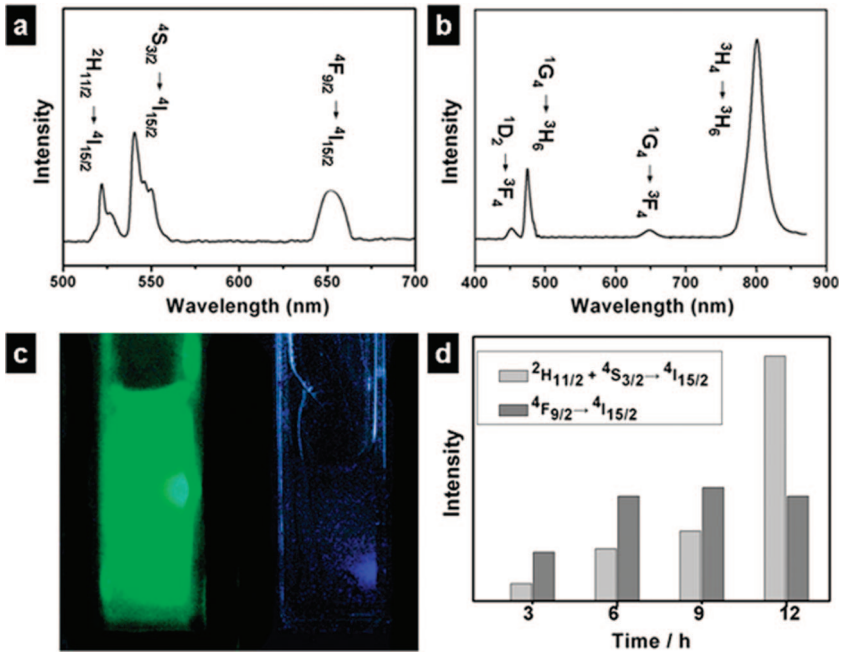

Figure 4. Spectroscopic characterization for upconversion luminescence. (a,b) Upconversion luminescence spectra of β-$NaYF_4$: 2% Er^{3+}, 20% Yb^{3+} (a) and β-$NaYF_4$: 2% Tm^{3+}, 20% Yb^{3+} (b) excited with a 978 nm laser diode (power density = 80 W/cm^2). (c) Photographs for the upconversion luminescence in 1 wt% hexane solution of β-$NaYF_4$: 2% Er^{3+}, 20% Yb^{3+} (1) and β-$NaYF_4$: 2% Tm^{3+}, 20% Yb^{3+} (2) excited with a laser power of 800 mW at 978 nm. (d) Integrated green upconversion emission intensity of a β-$NaYF_4$: 2% Er^{3+}, 20% Yb^{3+} phosphor as a function of the reaction time at 120 °C.

mation, the plots of unit cell volume per $NaMF_4$ molecule along the rare earth series are in agreement with the lanthanide contraction.

On the basis of the above results, we believe that the thermodynamic driving force should be a key to the formation of β-$NaYF_4$ *via* the hydrothermal *in situ* ion-exchange approach since the structure of the hexagonal $NaYF_4$ is more stable. For the hydrothermal *in situ* ion-exchange process, it is different from the classical thermodynamic or kinetic controlled crystallization process which is based predominantly on the modification of the activation energy barriers of nucleation, growth, and phase transformation.[29] During the hydrothermal *in situ* ion-exchange process, there is a minimal crystal structure reorganization which is different from classical crystallization that usually occurs by dissolution−renucleation processes. When HF diffuses into single-crystalline $Y(OH)_3$ nanotubes, F^- ions can substitute the OH^- ions and interact with Y^{3+} ions to form the more stable β-$NaYF_4$ phase on three types of sites (Supporting Information, Figure S8).[30,31] Furthermore, because in the hexagonal $NaYF_4$ crystals Na^+ ions are randomly dispersed in different sites (Supporting Information, Figure S8),[30,31] they, therefore, can be easily trapped into the crystals to form a more stable β-$NaYF_4$ phase under the thermodynamic driving force effect. The lattice constant in the *c*-axis is essentially unchanged during the hydrothermal *in situ* ion-exchange process since the hexagonal structural similarities (Supporting Information, Figure S9). As a result, the positions and arrangements of Y atoms in the parent remain unaffected during the transformation. It is this topotactic feature that leads to the formation of single-crystalline β-$NaYF_4$ nanotubes at low hydrothermal temperature, rather than the dissolution−renucleation processes described in the classical crystallization theories.[20,26,29,32]

The multicolor fluorescence can be observed in the Yb^{3+}/Er^{3+}(green) and Yb^{3+}/Tm^{3+}(blue) co-doped β-$NaYF_4$ nanotubes synthesized from the hydrothermal *in situ* ion-exchange method. The visible and NIR upconversion luminescence spectra of β-$NaYF_4$: 2% Er^{3+}, 20% Yb^{3+} and β-$NaYF_4$: 2% Tm^{3+}, 20% Yb^{3+} under infrared excitation (978 nm) are shown in Figure 4a,b, respectively. It corresponds to that for Er^{3+} and Tm^{3+} in β-$NaYF_4$ nanostructured materials reported previously.[33,34] The emission bands can be assigned to transitions within the 4f−4f levels of Er^{3+} and Tm^{3+} ions. In the Yb^{3+}/Er^{3+} co-doped β-$NaYF_4$ sample, green luminescence between 510 and 570 nm can be assigned to the ($^2H_{11/2}$, $^4S_{3/2}$) $\rightarrow {}^4I_{15/2}$ transition. A red emission is observed between 630 and 680 nm originating from the $^4F_{9/2} \rightarrow {}^4I_{15/2}$ transition. In comparison to the bulk samples,[35,36] the ratios of red to green emissions for β-$NaYF_4$: 2% Er^{3+}, 20% Yb^{3+} are very similar but different from the nanotube arrays we reported previously.[18] It may be ascribed to the mild hydrothermal reaction at low temperature to avoid the multiphonon relaxation effect and the effective F^- diffusion to avoid the oxygen contamination. In the case of Tm^{3+}, the visible luminescence originates from two stages: $^1G_4 \rightarrow {}^3H_6$ and $^1G_4 \rightarrow {}^3F_4$. The former results in a blue emission between 450 and 490 nm, and the latter yields a weak red emission between 630 and 680 nm. Furthermore, an intense NIR emission can be observed between 750 and 850 nm due to the $^3H_4 \rightarrow {}^3H_6$ transition. The mechanism responsible for the UC luminescence is shown in the schematic energy level diagrams (Supporting Information, Figure S10). Figure 4c shows photographs of eye-visible UC luminescence in hexane solutions of β-$NaYF_4$: 2% Er^{3+}, 20% Yb^{3+} and β-$NaYF_4$: 2% Tm^{3+}, 20% Yb^{3+} excited with a laser at 978 nm, indicating that the nanotubes are excellent UC hosts. The UC emission intensities and the ratios of the various emissions are influenced by the doping levels, excitation power, preparation temperature, and impurities.[33] Thereinto, the oxygen contamination effect is very important for the UC emission efficiency. As shown in Figure 4d, the green and red UC emission changes significantly with

time as the hydrothermal *in situ* ion-exchange reaction at 120 °C. The intensity of the red UC luminescence at 650 nm is always stronger than the green one, probably ascribed to the oxygen effect (Figure 2).[36,37] When the F-substituted reaction is carried out at 120 °C for 12 h (Figure 2), the green ($^2H_{11/2} + {}^4S_{3/2} \rightarrow {}^4I_{15/2}$) intensity surpasses red emission ($^4F_{9/2} \rightarrow {}^4I_{15/2}$) intensity, relating to low oxygen content. For the Yb^{3+}/Er^{3+} (green) co-doped β-$NaYF_4$ nanotubes, oxygen impurities can increase the multiphonon relaxation rates between the metastable states with the effect of reducing the overall visible emission intensity and enhancing the red to green emission ratios[35−37] in agreement with that from the previous reports. Therefore, the red to green emission ratio decreases as the oxygen decrease during the F-substituted process.

CONCLUSION

In summary, a successful synthesis of uniform rare earth fluoride β-$NaMF_4$ nanotubes is demonstrated *via* hydrothermal *in situ* ion-exchange reaction by using rare earth hydroxides [$M(OH)_3$] as a parent (where M = Y, Pr, Sm, Gd, Tb, Dy, Er, and their mixture). The shape, size, and single crystallinity of the template are retained with high fidelity. The single-crystal β-$NaMF_4$ nanotubes with uniform diameter (80−500 nm), aspect ratio (6−30), and wall thickness (25−80 nm) are easily obtained. The thermodynamic driving force is a key to the formation of β-$NaYF_4$ *via* the hydrothermal *in situ* ion-exchange approach. The lattice constant in *c*-axis is essentially unchanged during the ion-exchange process since the hexagonal structural similarities. The multicolor upconverison emission is realized with the rare earth doped fluorides. The red to green emission ratio decreases as the oxygen decreases during the F-substituted process. It is expected that these single-crystal rare earth fluoride nanotubes would have potential in applications as building blocks for many functional devices including solid-state laser, telecommucation fibers, and some other optics and sensors.

MATERIALS AND METHODS

Hydrothermal Synthesis of $M(OH)_3$ Nanotubes. Rare earth hydroxide nanotubes were hydrothermally prepared from their nitrates in the presence of alkali. For a typical synthesis, 5.0 mL of 0.85 M $Y(NO_3)_3$ from the high purity Y_2O_3 (99.99%) was added with 10 wt% NaOH solution until it reached pH 14, and the white precipitate was obtained. The colloidal precipitate was transferred into a stainless Teflon-lined autoclave (40 mL) and heated at 120 °C for 12 h. After cooling to room temperature, the product was collected, washed with water, and dried at 80 °C for 3 h in air.

Synthesis of Rare Earth Fluoride Nanotube. In a typical synthesis, 0.38 g of NaF and 0.65 g of HF (40%) were dissolved in 25 mL of deionized water with stirring for 30 min, then 0.3 g of $Y(OH)_3$ nanotubes prepared as above was added into the mixture solution. Finally, the mixture solution was transferred into a stainless-steel autoclave and heated at 120 °C for 12 h. After cooling, the powder sample was washed with deionized water and ethanol several times and dried at 80 °C for 2 h in a vacuum oven.

Characterization. X-ray diffraction (XRD) patterns were recorded on a Bruker D4 X-ray diffractometer with Ni-filtered Cu KR radiation (40 kV, 40 mA). Transmission electron microscopy (TEM) measurements were conducted on a JEOL 2011 microscope operated at 200 kV. All samples were first dispersed in ethanol and then collected using copper grids covered with carbon films for measurements. Energy dispersive X-ray spectroscopy (EDX) was performed on a JEOL 2010 EDX instrument. Scanning electron microscopy (SEM) images were taken with a Philips XL30 electron microscope operating at 20 kV. A thin film of gold was sprayed on the sample before this characterization. Upconversion luminescent spectra were measured on an optical spectrum analyzer (ANDO AQ6317, Japan). The sample was put in a curet with 1.0 cm path-length and was excited by a 978 nm CW semiconductor diode laser (P_{max} = 800 mW at 1000 mA). The upconversion luminescence spectra were collected by a multimode optical fiber with 0.6 mm core diameter on an optical spectrum analyzer. The distance between the top of the fiber and the sample was about 2 mm.

Acknowledgment. This work was supported by the NSF of China (20721063 and 20521140450), the State Key Basic Research Program of the PRC (2006CB0N0302), the Shanghai Science & Technology Committee (06DJ14006), and Shanghai Leading Academic Discipline Project, Project Number B108.

Supporting Information Available: XRD, SEM, and TEM analysis of the $NaMF_4$ (such as Re = Pr, Sm, Gd, Tb, Dy, Er, as well as lanthanide-doped rare earth $NaMF_4$) prepared at different reaction conditions, plots of the measured lattice volume over the number of $NaMF_4$ molecules (Z) in one unit cell against the rare earth series, optimal experimental conditions and morphologies of $M(OH)_3$ and β-$NaMF_4$ nanotubes, and schematic energy level diagrams of the Er^{3+}, Tm^{3+}, and Yb^{3+} dopant ions and upconversion mechanism. This material is available free of charge *via* the Internet at http://pubs.acs.org.

REFERENCES AND NOTES

1. Xia, Y. N.; Yang, P. D.; Sun, Y. G.; Wu, Y. Y.; Brian, M.; Byron, G.; Yin, Y. D.; Franklin, K.; Yan, H. Q. One-Dimensional Nanostructures: Synthesis, Characterization, and Applications. *Adv. Mater.* **2003**, *15*, 353–389.
2. Huang, M. H.; Mao, S.; Feick, H.; Yan, H. Q.; Wu, Y. Y.; Kind, H.; Weber, E.; Russo, R.; Yang, P. D. Room-Temperature Ultraviolet Nanowire Nanolasers. *Science* **2001**, *292*, 1897–1899.
3. Rumbles, G. Solid-State Optics: A Laser That Turns Down the Heat. *Nature* **2001**, *409*, 572–573.
4. Wang, E. W.; Sheehan, P. E.; Lieber, C. M. Nanobeam Mechanics: Elasticity, Strength, and Toughness of Nanorods and Nanotubes. *Science* **1997**, *277*, 1971–1975.
5. Hicks, L. D.; Dresselhaus, M. S. Thermoelectric Figure of Merit of a One-Dimensional Conductor. *Phys. Rev. B* **1995**, *47*, 16631–16634.
6. Hu, J.; Odom, T. W.; Lieber, C. M. Chemistry and Physics in One Dimension: Synthesis and Properties of Nanowires and Nanotubes. *Acc. Chem. Res.* **1999**, *32*, 435–445.
7. Wu, Y.; Yang, P. D. Direct Observation of Vapor-Liquid-Solid Nanowire Growth. *J. Am. Chem. Soc.* **2001**, *123*, 3165–3166.
8. Chen, C. C.; Yeh, C. C. Large-Scale Catalytic Synthesis of Crystalline Gallium Nitride Nanowires. *Adv. Mater.* **2000**, *12*, 738–741.
9. Yazawa, M.; Koguchi, M. H.; Muto, M.; Ozawa, M.; Hiruma, H. Effect of One Monolayer of Surface Gold Atoms on the Epitaxial Growth of InAs Nanowhiskers. *Appl. Phys. Lett.* **1992**, *61*, 2051–2053.
10. Auzel, F. Upconversion and Anti-Stokes Processes with f and d Ions in Solids. *Chem. Rev.* **2004**, *104*, 139–174.

11. Downing, E.; Hesselink, L.; Ralston, J.; Macfarlane, R. A. A Three-Color, Solid-State, Three-Dimensional Display. *Science* **1996**, *273*, 1185–1189.
12. Van, D.; Rijke, F.; Zijlmans, H.; Li, S.; Vail, T.; Raap, A. K. Up-Converting Phosphor Reporters for Nucleic Acid Microarrays. *Nat. Biotechnol.* **2001**, *19*, 273–276.
13. Heer, S.; Kompe, K.; Gudel, H. U.; Haase, M. High-Quality Sodium Rare-Earth Fluoride Nanocrystals: Controlled Synthesis and Optical Properties. *Adv. Mater.* **2004**, *16*, 2102–2105.
14. Yi, G. S.; Lu, H. C.; Zhao, S. Y.; Yue, G.; Yang, W. J. Synthesis, Characterization, and Biological Application of Size-Controlled Nanocrystalline $NaYF_4$:Yb, Er Infrared-to-Visible Up-Conversion Phosphors. *Nano. Lett.* **2004**, *4*, 2191–2196.
15. Mai, H. X.; Zhang, Y. W.; Si, R.; Yan, Z. G.; Yan, C. H. High-Quality Sodium Rare-Earth Fluoride Nanocrystals: Controlled Synthesis and Optical Properties. *J. Am. Chem. Soc.* **2006**, *128*, 6426–6436.
16. Boyer, J. C.; Vetrone, F.; Cuccia, L. A.; Capobianco, J. A. Synthesis of Colloidal Upconverting $NaYF_4$ Nanocrystals Doped with Er^{3+}, Yb^{3+} and Tm^{3+}, Yb^{3+} *via* Thermal Decomposition of Lanthanide Trifluoroacetate Precursors. *J. Am. Chem. Soc.* **2006**, *128*, 7444–7445.
17. Wang, X.; Zhuang, J.; Peng, Q.; Li, Y. D. A General Strategy for Nanocrystal Synthesis. *Nature* **2005**, *437*, 121–124.
18. Zhang, F.; Wan, Y.; Ying, T.; Zhang, F. Q.; Shi, Y. F.; Xie, S. H.; Li, Y. G.; Xu, L.; Tu, B.; Zhao, D. Y. Uniform Nanostructured Arrays of Sodium Rare-Earth Fluorides for Highly Efficient Multicolor Upconversion Luminescence. *Angew. Chem., Int. Ed.* **2007**, *46*, 7976–7979.
19. Liang, L. F.; Xu, H. F.; Su, Q.; Konishi, H.; Jiang, Y. B.; Wu, M. M.; Wang, Y. F.; Xia, D. Y. Hydrothermal Synthesis of Prismatic $NaHoF_4$ Microtubes and $NaSmF_4$ Nanotubes. *Inorg. Chem.* **2004**, *43*, 1594–1596.
20. Zhuang, J. L.; Liang, L. F.; Sung, H. H. Y.; Yang, X. F.; Wu, M. M.; Williams, I. D.; Feng, S. H.; Su, Q. Controlled Hydrothermal Growth and Up-Conversion Emission of $NaLnF_4$ (Ln) Y, Dy-Yb). *Inorg. Chem.* **2007**, *46*, 5404–5410.
21. Xiong, Y. J.; Mayers, B. T.; Xia, Y. N. Some Recent Developments in the Chemical Synthesis of Inorganic Nanotubes. *Chem.Commun.* **2005**, *15*, 5013–5022.
22. Chen, Q.; Zhou, W. Z.; Du, G. H.; Peng, L. M. Trititanate Nanotubes Made *via* a Single Alkali Treatment. *Adv. Mater.* **2002**, *14*, 1208–1211.
23. Zhang, S.; Peng, L. M.; Chen, Q.; Du, G. H.; Dawson, G.; Zhou, W. Z. Formation Mechanism of $H_2Ti_3O_7$ Nanotubes. *Phys. Rev. Lett.* **2003**, *91*, 250163-1–250163-4.
24. Du, N.; Zhang, H.; Chen, B. D.; Ma, X. Y.; Liu, Z. H.; Wu, J. B.; Yang, D. R. Porous Indium Oxide Nanotubes: Layer-by-Layer Assembly on Carbon-Nanotube Templates and Application for Room-Temperature NH_3 Gas Sensors. *Adv. Mater.* **2005**, *17*, 3005–3009.
25. Steinhart, M.; Wendorff, J. H.; Greiner, A.; Wehrspohn, R. B.; Nielsch, K.; Schilling, J.; Choi, J.; Gosele, U. Polymer Nanotubes by Wetting of Ordered Porous Templates. *Science* **2002**, *296*, 1997.
26. Ding, S.; Lu, P.; Zheng, J. G.; Yang, X. F.; Zhao, F. L.; Chen, J.; Wu, H.; Wu, M. M. Textured Tubular Nanoparticle Structures: Precursor-Templated Synthesis of GaN Sub-micrometer Sized Tubes. *Adv. Funct. Mater.* **2007**, *17*, 1879–1886.
27. Fang, Y. P.; Xu, A. W.; You, L. P.; Song, R. Q.; Yu, J. C.; Zhang, H. X.; Li, Q.; Liu, H. Q. Hydrothermal Synthesis of Rare Earth (Tb, Y) Hydroxide and Oxide Nanotubes. *Adv. Funct. Mater.* **2003**, *13*, 955–960.
28. Wang, X.; Sun, X. M.; Yun, D. P.; Zou, B. S.; Li, Y. D. Rare Earth Compound Nanotubes. *Adv. Mater.* **2003**, *15*, 1442–1445.
29. Chen, Y.; Johnson, E.; Peng, X. Formation of Monodisperse and Shape-Controlled MnO Nanocrystals in Non-injection Synthesis: Self-Focusing *via* Ripening. *J. Am. Chem. Soc.* **2007**, *129*, 10937–10947.
30. Thoma, R. E.; Insley, H.; Hebert, G. M. The Sodium Fluoride-Lanthanide Trifluoride Systems. *Inorg. Chem.* **1966**, *5*, 1222–1229.
31. Aebischer, A.; Hostettler, M.; Hauser, J.; Kramer, K.; Weber, T.; Gudel, H. U.; Burgi, H. B. Structural and Spectroscopic Characterization of Active Sites in a Family of Light-Emitting Sodium Lanthanide Tetrafluorides. *Angew. Chem., Int. Ed.* **2006**, *45*, 2802–2806.
32. Jeong, U. Y.; Camargo, P. H. C.; Lee, Y. H.; Xia, Y. N. Chemical Transformation: A Powerful Route to Metal Chalcogenide Nanowires. *J. Mater. Chem.* **2006**, *16*, 3893–3897.
33. Stouwdam, J. W.; Van Veggel, F. J. M. Near-infrared Emission of Redispersible Er^{3+}, Nd^{3+}, and Ho^{3+} Doped LaF_3 Nanoparticles. *Nano. Lett.* **2002**, *2*, 733–737.
34. Schafer, H.; Ptacck, P.; Kompe, K.; Hasse, M. Lanthanide-Doped $NaYF_4$ Nanocrystals in Aqueous Solution Displaying Strong Up-Conversion Emission. *Chem. Mater.* **2007**, *19*, 1396–1400.
35. Kramer, K. W.; Biner, D.; Frei, G.; Gudel, H. U.; Hehlen, M. P.; Luthi, S. R. Hexagonal Sodium Yttrium Fluoride Based Green and Blue Emitting Upconversion Phosphors. *Chem. Mater.* **2004**, *16*, 1244–1251.
36. Zhang, J. S.; Qin, W. P.; Zhao, D.; Hu, D. G. J.; Zhang, J. H.; Wang, Y.; Cao, C. Y. Spectral Variations and Energy Transfer Processes on Both Er^{3+} Ion Concentration and Excitation Densities in $Yb^{3+}-Er^{3+}$ Codoped LaF_3 Materials. *J. Lumin.* **2007**, *122*, 506–508.
37. Sivakumar, S.; van Veggel, F. J. M.; Stanley, P. Near-Infrared (NIR) to Red and Green Up-Conversion Emission from Silica Sol−Gel Thin Films Made with $La_{0.45}Yb_{0.50}Er_{0.05}F_3$ Nanoparticles, Hetero-Looping-Enhanced Energy Transfer (Hetero-LEET): A New Up-Conversion Process. *J. Am. Chem. Soc.* **2007**, *129*, 620–625.